# Application of the Method of Moment and Monte-Carlo Simulation to Extract Oil Spill Areas from Synthetic Aperture Radar Images

Tae-Ho Kim, Chan-Su Yang
Department of Ocean Environmental System Science
University of Science and Technology, UST
Daejeon, Republic of Korea
{thkim,yangcs}@kiost.ac

Kazuo Ouchi
Korea Ocean Satellite Center
Korea Institute of Ocean Science and Technology, KIOST
Ansan, Republic of Korea
Ouchi_sar@yahoo.co.jp

Yisok Oh
Department of Electronics, Information and Communication Engineering
Hongik University
Seoul, Republic of Korea
yisokoh@hongik.ac.kr

***Abstract*— Synthetic aperture radar (SAR) is a useful instrument to detect oil slicks on the sea surface. Generally, the algorithm for detection of oil slick in SAR images is based on the approach to distinguish the darker area compared to the surrounding area defined on the typical backscatter level. This value can calculate by scattering model using moment method and Monte-Carlo simulation for various conditions of surface roughness induced wind, oil-layer thickness, frequency, polarization and incidence angle. For the simulation, Automatic Weather System (AWS) were used to generate wind fields in SAR image area. The purpose of this study is that extraction of oil spill area from SAR images. For the extraction, radar backscattering value was calculated using scattering model, and it is used by threshold value for distinguishing between oil-covered and non-area in SAR images. In this study, oil thickness assumed by constant, and didn't take into account the direction of the wind. From this study results, we expect that automatic classification of oil slick features from lookalikes and detecting of seepage on sea surface.**

***Keywords—Oil Spill; Numerical Simulation; Method of moment; Monte-Carlo simulation; Satellite remote sensing; Hebei Spirit***

## I. INTRODUCTION

Remote sensing using airborne and spaceborne sensors is a most efficient technique for monitoring oil slicks on a regional as well as global scale, and much effort has been made for accurate detection, identification and classification of oil-covered surface [1], [2], [3], [4], [5], [6]. In the recent cases, for example, a large number of airborne and spaceborne imagery have been acquired and analyzed for the 2007 *Hebei Spirit* oil spill in the Yellow Sea [7], [8], [9] and 2011 Deepwater Horizon oil spill in the Gulf of Mexico [10], [11], [12], [13]. SAR has all-weather and day-and-night imaging capability [14]. The imaging mechanism of oil slicks by SAR is based on the difference in surface roughness. Oil slick on the sea surface damps short gravity-capillary surface waves, and thus, reduces the radar backscatter [3], [5], [8], [15], [16]. In SAR images, the oil-covered surface appears as dark features [17]. Generally, the algorithm for detection of oil slick in SAR images is based on the approach to distinguish the areas of small image intensity values by thresholding [1].

The main problem in oil spill detecting is that it is difficult to identify the oil-covered surface from lookalike surfaces under low to no wind, rain cells, upwelling, and biogenic slicks, since the images of both surfaces appear dark with similar radar cross section. Several techniques have been proposed to identify oil slick features from lookalikes using image classification algorithms, such as those based on fuzzy logic, neural network, and polarimetric analyses [6], [12]. In this paper, preliminary results are presented the oil slick extraction in SAR image using moment method and Monte-Carlo simulation in the 2007 *Hebei Spirit* case.

## II. *HEBEI SPIRIT* OIL TANKER ACCIDENT AND SATELLITE DATA

### A. *Hebei spirit oil tanker accident*

On December 7, 2007 at local time (LT) 07:15 (UTC 22:15, December 6), the oil tanker *Hebei Spirit* collided with a crane vessel about 8 km off the coast of Taean in the west of the Korea (approximate location: 36˚ 49.93'N, 126˚ 2.46'), spilling approximately 10,900 tons of crude oil [9]. The oil spill was stopped at about 07: 30, December 9 (LT). At the time of collision, the sea state was high with wind speed and significant waveheight of approximately 14 m/s and 3-5 m, respectively.

## B. Satellite data

After the incident, several images were acquired using spaceborne platforms from 8th to 25th December 2007. In this study, 4 SAR images acquired by ENVISAT-ASAR, RADARSAT-1, and TerraSAR-X were used for comparison with the simulation results. The radiometric calibration and geometric correction were performed to calculate normalized radar cross section (NRCS), and Fig. 1 illustrates the geocoded SAR images, and TABLE I shows the data acquisition time, sensor mode, polarization, swath width, spatial resolution, wind direction, and wind at the AWS stations closest to the centroid of the slick areas at each satellite data acquisition time. It should be noted that the dark areas in the inland sea and south coast of Taean Peninsula seen in Figure 1b, 1c and 1d were wind-sheltered areas, but not covered by oil slicks. As mentioned previously, it is difficult to distinguish wind-sheltered lookalikes and oil-covered surfaces by SAR without *in-situ* data or appropriate processing methods of image classification.

## C. Extraction of oil slicks in SAR images

The areas covered by oil slicks were extracted in the SAR images by thresholding. The threshold value (in decibels) was used to identify the dark spots in processed SAR images and it was computed using numerical scattering model depending on the radar parameters, target parameters and environmental parameter related to each SAR image. In order to consider reduction effect for surface roughness, damping ratio has been theoretically calculated. The formulation is given as follow [8]:

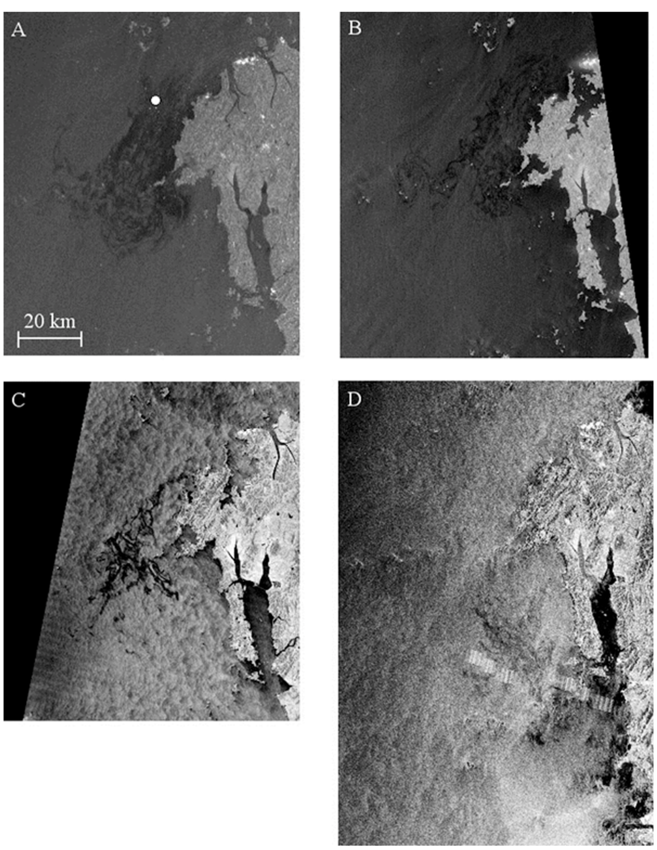


Fig. 1. SAR images including oil slicks.

$$\frac{W_s(k)}{W_w(k)} = \frac{\beta_w \quad 2c_g \Delta_w + \alpha_w}{\beta_s - 2c_g \Delta_s + \alpha_s} \tag{1}$$

where $W_{w,s}(k)$ is the sea surface roughness spectrum; $\beta_{w,s}$ is the wind wave growth rate; $c_g$ is the wave group velocity; $\Delta_{w,s}$ is the viscous damping coefficient; $\alpha_{w,s}$ is the nonlinear energy transfer rate; the subscript w and s represent to the seawater and oil slick respectively. Each parameter and physical-chemical properties of oil slick are estimated by [15]. They were used to distinguish region of interest (ROI), which includes oil slicks and lookalikes. Oil slick areas were determined by the histograms of NRCS in ROI and visual inspection on the basis of reports from Central Disaster and Safety Countermeasures Headquarters.

# III. WIND FIELD FROM AWS

Wind data were obtained from 19 AWS stations at different heights around the position of collision. The data contain the wind speed and direction averaged over 1 minute at 1 minute interval. Hellman exponential law was used to convert the measured wind speed to the wind speed at 10 m height, and it is defined as follows [39]:

$$U(z) = U(z_a) \times (z / z_a)^{\alpha} \tag{2}$$

where $U(z)$ is the wind speed to the height z, and $U(z_a)$ is the wind speed to the height $z_a$ which is referred to as the 10 meters height in this study. $\alpha$ is the friction coefficient or Hellman exponent which is a function of the topography and roughness at a measurement site. If the site characteristics are yet to be determined, a value of 0.14 is a good first approximation [18], [19]. This value was used to convert the wind speed at 10 meter height, and the wind speed and direction were averaged during 30 minutes at each AWS station. Wind field at grid spacing of 500 m was generated by the same as for the current data using linear interpolation and the method of nearest neighbor (Fig. 2).

**TABLE I.** Parameters of satellite sensors and wind data at the AWS stations closest to the centroid of the slick areas at each satellite data acquisition time.

| **Satellite** | ENVISAT ASAR | RADARSAT-1 | TerraSAR-X | ENVISAT ASAR |
|---|---|---|---|---|
| **Acquisition time (LT)** | 2007.12.11 10:40 | 2007.12.11 18:31 | 2007.12.13 06:44 | 2007.12.14 10:45 |
| **Mode / Polarization** | Wide Swath / VV | Wide / HH | ScanSAR / VV | Wide Swath / VV |
| **Incidence angle [deg]** | 31.0 - 36.3 | 31 - 39 | 31.8 – 40.5 | 19.2 – 26.7 |
| **Swath width [km]** | 405 | 150 | 100 | 405 |
| **Nominal resolution [m] (range/azimuth)** | 150 / 150 | 25 / 27 | 18.5 / 18.5 | 150 / 150 |
| **Wind speed [m/s]** | 5.6 | 6.3 | 4.3 | 6.9 |
| **Wind direction [degrees]** | 338.0 | 347.0 | 323.1 | 339.0 |

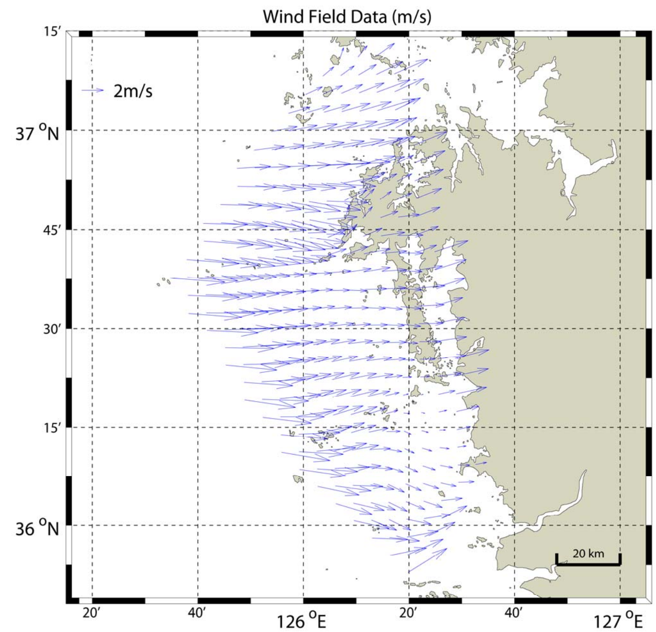


Fig. 2. Wind field around oil slick area.

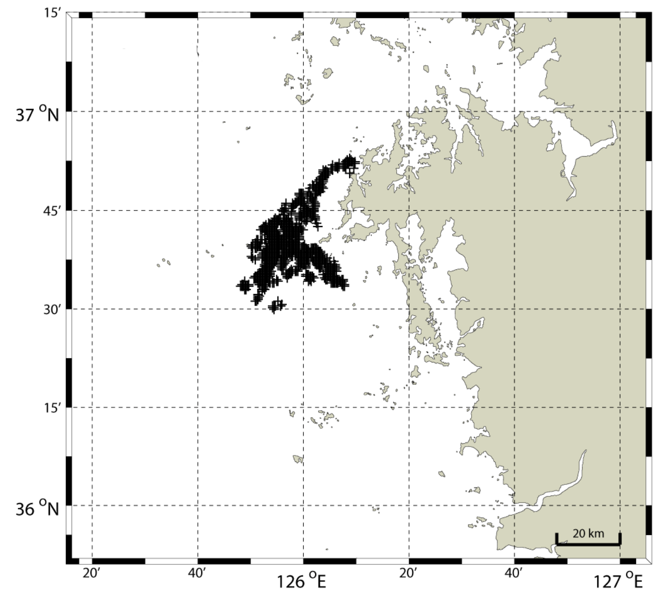


Fig. 3. Example of extraction oil spill area from TerraSAR-X (Fig. 1C).

## IV. Result and Conclusions

Oil slicks on SAR image appear as dark features, and it can distinguish by radar backscattering value. In this study, the oil spill areas from SAR images were extracted by the threshold value. In order to calculate the threshold value, numerical scattering model depending on the radar, target and environmental parameters was performed, and the model is based on method of moment and Monte-Carlo simulation. Fig. 3 represent example of extraction oil slick area from SAR image (Fig. 1C). It is shows good agreement with SAR image.

The main problem in oil spill and seepages detection is that it is difficult to identify the oil slicks on the surface from look-alike surfaces, such as under low to no wind, rain cells, upwelling, and biogenic slicks, since the images of both surfaces appear dark with similar radar cross section. Using successive satellite images and numerical simulation, therefore, mechanism to distinguish between oil slicks and look-alike features will develop.

Present study only applied to oil spill case by ship accident.. However, the subsurface oil, such as destruction of the Deepwater Horizon drilling platform or seepages from underground, release caused the spill to interact with the marine environment that was different from that observed in surface spills. Using this method, therefore, further research to detect the oil spill from seabed will carry out.


## Acknowledgment

The satellite data were provided by Korea Aerospace Research Institute (KOMPSAT-2), Canada RADARSAT-1 (Canadian Space Agency/ RADARSAT International), European Space Agency (ESA), and German Aerospace Center (TerraSAR-X).


## References


[1] C. Brekke and A. H. S. Solberg, “Oil spill detection by satellite remote sensing,” Remote Sens. Environ., vol. 95(1), pp. 1-13, 2005.

[2] M. F. Fingas and C. E. Brown, “Review of oil spill remote sensing,” Spill Sci. Technol. Bull., vol. 4(4), pp. 199-208, 1997.

[3] M. Migliaccio, M. Tranfaglia and S. A. Ermakov, “A physical approach for the observation of oil spills in SAR images,” IEEE J. Ocean Eng., vol. 30(3), pp. 496-507, 2005.

[4] M. Migliaccio, A. Gambardella and M. Tranfaglia, “SAR polarimetry to observe oil spills,” IEEE Trans. Geosci. Remote Sens., vol. 45(2), pp. 506-511, 2007.

[5] F. Nirchio, M. Sorgente, A. Giancaspro, W. Biamino, E. Parisato, R. Ravera and P. Trivero, “Automatic detection of oil spills from SAR images,” Int. J. Remote Sens., vol. 26 (6), pp. 1157-1174, 2005.

[6] K. N. Topouzelis, “Oil spill detection by SAR images: dark formation detection, feature extraction and classification algorithms,” Sensors, vol. 8(10), pp. 6642-6659, 2008.

[7] C. S. Yang, D. Kim and J. H. Oh, “Study on improvement of oil spill prediction using satellite data and oil-spill model: Hebei Spirit Oil Spill,” Kor. J. Remote Sens., vol. 25(5), pp. 435-444, 2009. (in Korean)

[8] C. S. Yang, S. M. Park, Y. Oh Y and K. Ouchi, “An analysis of the radar backscatter fromoil-covered sea surfaces usingmomentmethod andMonte-Carlo simulation: preliminary results,” Acta Oceanol. Sin., vol. 32(1), pp. 59-67, 2013.

[9] U. H Yim, M. Kim, S. Y. Ha, S. Kim and W. J. Shim, “Oil spill environmental forensics: the Hebei Spirit oil spill case,” Environ. Sci. Tech., vol. 46(12), pp. 6431-6437, 2012.

[10] A. J. Mariano, V. H. Kourafalou, A. Srinivasan, H. Kang, G. R. Halliwell, E. H. Ryan and M. Roffer, “On the modeling of the 2010 Gulf of Mexico oil spill,” Dyn. Atmos. Oceans, vol. 52(1), pp. 322-340, 2011.

[11] J. C. Dietrich, C. J. Trahan, M. T. Howard, J. G. Fleming, R. J. Weaver, S. Tanaka, L. Yu, R. A. Jr. Luettich, C. N. Dawson, J. J. Westerink, G. Wells, A. Lu, K. Vega, A. Kubach, K. M. Dresback, R. L. Kolar, C. Kaiser and R. R. Twilley, “Surface trajectories of oil transport along the Northern Coastline of the Gulf of Mexico,” Cont. Shelf Res., vol. 41, pp. 17-47, 2012.

[12] I. Leifer, W. J. Lehr, D. Simecek-Beatty, E. Bradley, R.Clark, P. Dennison, Y. Hu, S. Matheson, C. E. Jones, B. Holt, M. Reif, D. A. Roberts, J. Svejkovsky, G. Swayze and J. Wozencraft, “State of the art satellite and airborne marine oil spill remote sensing: Application to the

BP *Deepwater Horizon* oil spill," Remote Sens. Environ., vol. 124, pp. 185-209, 2012.

[13] Y. Liu, R. H. Weisberg, C. Hu and L. Zheng, "Tracking the Deepwater Horizon oil spill: A modeling perspective," EOS, vol. 92(6), pp. 45-52, 2011.

[14] K. Ouchi, "Recent Trend and Advance of Synthetic Aperture Radar with Selected Topics," Remote Sens., vol. 5(2), pp. 716-807, 2013.

[15] W. Alpers and H. Huhnerfuss, "The damping of ocean waves by surface films: A new look at an old problem," J. Geophys. Res., vol. 94(C5), pp. 6251-6265, 1989.

[16] M. Gade, W. Alpers, H. Huhnerfuss, H. Masuko and T. Kobayashi, "Imaging of biogenic and anthropogenic ocean surface films by the multifrequency/multipolarization SIR-C/X-SAR," J. Geophys. Res., vol. 103(C9), pp. 18851-18866, 1998.

[17] D. J. Kim, W. M. Moon and Y. S. Kim, "Application of TerraSAR-X data for emergent oil-spill monitoring," IEEE Trans. Geosci. Remote Sens., vol. 48(2), pp. 852-863, 2010.

[18] F. Bañuelos-Ruedas, C. Á. Camacho and S. Rios-Marcuello, "Methodologies Used in the Extrapolation of Wind Speed at Different Heights and Its Impact in the Wind Energy Resource Assessment in a Region," in Wind Farm - Technical Regulations, Potential Estimation and Siting Assessment, G. O. Suvire, Eds. Croatia: InTech, 2011. Available: http://www.intechopen.com/books/wind-farm-technical-regulations-potential-estimation-and-siting-assessment. Accessed 17 July 2013.

[19] RETScreen Software Online User Manual. Available: http://www.retscreen.net/download.php/ ang/440/0/PSH3.pdf . Accessed 17 July 2013.